SUPPLEMENTAL INFORMATION

1> Supplementary Materials and Methods (Page 2 to Page 7)

2> Supplementary References (Page 8)

3> Supplementary Tables: (Page 9 to Page 15)

+ Table S1. The target sequences for siRNAs

+ Table S2. TaqMan gene expression assays used for qPCR analysis

+ Table S3. List of antibodies used for IP and IB analysis

+ Table S4. List of proteins used for *in vitro* kinase assay

+ Table S5. Characteristics of patient samples

+ Table S6. Mathematical model parameters and initial conditions

4> Supplementary Figures Legends (Page 15 to Page 18)

+ **Figure S1.** Specificity of SmartFlare probes

+ **Figure S2.** Effects of AC220 treatment *in vivo* on levels of miR-126 and miR-155

+ **Figure S3.** Effects of AC220 and K118-SHIP1 inhibitor on levels of miR-126 and apoptosis

+ **Figure S4.** Effects of AKT phosphorylation on SPRED1 stabilization and localization

+ Figure S5. Effects of FLT3 activation on miR-155-regulated miR-126 levels

+ Figure S6. Schematic model of FLT3-ITD-caused a deregulated “circuitous architecture” of the miRNome in AML

5> Supplementary Figures

Supplementary Materials and Methods

In vivo treatment of normal and miR-155 KO mice and isolation of cells from bone marrow

The WT B6 and miR-155 KO mice were treated with 25 mg/kg LPS from P. aeruginosa (Sigma, #8643) via IP (26-gauge needle). The mice were euthanized after 24 hours of treatment. Tibias, femurs, and pelvis were excised. After removing the muscle and connective tissue, the bones were flushed five times using a 23-gauge needle and 3 ml of cold Iscove's modified Dulbecco's medium (IMDM) and collected as central marrow. Lin- cells were enriched through the lineage depletion kit from Miltenyi Biotec (#130-090-858) and used for *in vitro* analysis. Mouse care and experimental procedures were performed in accordance with federal guidelines and protocols and were approved by the Institutional Animal Care and Use Committee at the City of Hope.

Cell cultures, Plasmid and Chemicals

Mouse wt $Lin^{-}Sca\text{-}1^{+}c\text{-}Kit^{+}$ (LSK) cells were cultured in IMDM medium with 20% FBS, supplemented with 10ng/ml mouse SCF and 10ng/ml mouse TPO. All cells were cultured at 37°C with 5% CO_2 and high humidity. MV-4-11, THP1 and HL-60 cells were purchased from the American Type Culture Collection and maintained in IMDM (Iscove's Modified Dulbecco's Medium) or RPMI (Roswell Park Memorial Institute) medium supplemented with 10% FBS and 100 units of penicillin/streptomycin at 37°C with 5% CO_2. Cell lines were authenticated by cell morphology monitoring, growth curve analysis, and mycoplasma detection using a Mycoplasma detection kit (Roche, Germany).

GFP-SPRED1 and mutants were cloned in our laboratory using pcDNA vector (Invitrogen, Carlsbad, CA). AKT and HA-Ub constructs were from Dr. Jee-Yin Ahn (Sungkyunkwan University, South of Korea). AC220 was purchased from LC Laboratories (Woburn, MA). Lipopolysaccharides (LPS) was from Sigma (Saint Louis, MO). K118 (SHIP1 Inhibitor) was from Echelon (Salt Lake, UT). MG132 was from Selleckchem (Houston, TX).

Mononuclear cells isolation from patient samples

The specimen was transferred to a 50 ml conical tube and the volume was brought up to 25 ml using warm DPS (1x) with 2% FBS. The specimen was layered on the top of 20 ml Ficoll-Paque Plus in a 50 ml conical tube. Then, the tube was centrifuged at 300g for 32 minutes without break. The layer containing PBMC and plasma was carefully transferred to a 50 ml conical tube and the volume was brought up to 50 ml with warm DPS (1x). The tube was then centrifuge at 2400 rpm for 8 minutes. After discard the supernatant, the pellet was resuspended in 10 ml of warm DPBS (1x). The cell number and viability were determined, and the sample was frozen.

Synthetic small interfering RNA (siRNA) oligonucleotides

The siGENOME SMARTpool for si-RNA of AKT was purchased from Thermo Scientific (Lafayette, CO). Scrambled control RNA (siSCR) was used as a control. The target sequences for siRNAs are shown in Table S1.

q-PCR analysis

To measure the miRNA expression, total RNA was extracted using the miRNeasy Mini Kit (Qiagen, Valencia, CA). Reverse transcription using MultiScribe™ Reverse Transcriptase and q-PCR analysis using Taqman assays (Applied Biosystems) were performed according to the manufacturer's protocol. RNU44 and snoRNA234 was used as internal controls for human and mouse miRNA respectively. TaqMan gene expression assays used for qPCR analysis are listed in Table S2. Results are presented as log2-transformed ratio according to the $2^{-\Delta Ct}$ method (ΔCt=Ct of target –Ct of reference).

Flow cytometry analyses

Mouse cells were obtained from BM (from both tibias and femurs). For analysis of stem and progenitor cells, c-kit$^+$ cells were selected using anti-mouse CD117 microbeads or Lin$^-$ cells were

selected using Lineage depletion microbeads (both from Miltenyi Biotec, San Diego, CA). Stem and progenitor populations were identified as LSK cells ($Lin^{-}Sca\text{-}1^{hi}c\text{-}Kit^{hi}$) (1). All analyses were performed on a LSRII flow cytometer (BD Biosciences) and sorting was performed on ARIAIII or ARIA SORP instruments (BD Biosciences).

Lentiviral transduction of mouse cells

Mouse BM LSKs or Lin- were cultured overnight in IMDM with 20% FBS supplemented with 10ng/ml mouse IL3, IL6, SCF and TPO. Normal BM LSK or Lin- cells were transduced with FLT3-ITD or control retroviral supernatant (MOI=5) with polybrene (5 μg/ml, American Bioanalytical) by spinoculation, and 20-30% of GFP^{+} cells were detected at 48 h. GFP^{+} cells from the samples with low transduction efficiency (<80%) were selected by flow cytometry at 48h for further studies.

Apoptosis assay

Apoptosis was measured by labeling cells with Annexin V-PE or FITC or APC and 4, 6-diamidino-2-phenylindole (DAPI) (all from BD-PharMingen, San Diego, CA) and analyzed by flow cytometry.

Immunoprecipitation and Immunoblotting analyses

Cells were washed and harvested in ice-cold PBS and subsequently lysed in RIPA buffer containing 10 mM protease inhibitor cocktail (Thermo Scientific, Lafayette, CO). For immunoprecipitation, 500 μg – 1 mg of cell lysate were incubated with indicated antibody for overnight at 4°C. 50 μl of Protein A/G agarose beads (Cell Signaling, Danvers, MA) were added and the mixture was inverted for 3 hours at 4°C. For immunoblotting, immunoprecipitated complex or 50 μg of each cell lysate was separated on NuPAGE 4-12% gradient gels (Invitrogen, Carlsbad, CA) and immunocomplexes were visualized with enhanced chemiluminescence reagent (Thermo Scientific, Lafayette, CO). The list of antibodies is presented in Table S3.

Immunocytochemistry

Cells were collected, washed in ice-cold PBS and mounted on glass slide using the Cytocentrifuge (CytoSpin4, 600 rpm, 10 minutes). Cells then were washed with PBS, fixed in 4% paraformaldehyde for 15 minutes and permeabilized in 0.5% Triton X-100 for 15 minutes. Non-specific epitopes were blocked with 5% bovine serum albumin (BSA) for 30 minutes. Primary antibodies are listed in Table S3 and secondary anti-mouse/rabbit/goat-Alexa 594/488/647 goat antibodies were from Thermo Scientific (Lafayette, CO). Cell images were acquired using a Zeiss confocal laser-scanning-microscope (Zeiss LSM880). Nuclei were counterstained with prolong Gold Antifade with DAPI (Molecular Probes, Invitrogen, Carlsbad, CA).

Cellular Fractionation

The cells were collected and washed in PBS followed by fractionation into nuclear and cytoplasmic fractions using a subcellular fractionation kit (Thermo Scientific, Lafayette, CO). Briefly, the cells were vigorously vortexed in cytoplasmic extraction reagents and subsequently centrifuged to isolate the soluble cytoplasmic fraction. The remaining insoluble fraction, which contained nuclei, was suspended in nuclear extraction reagent and centrifuged to collect the nuclear fraction. All steps were performed at 4°C.

Kinase assay

One microgram of purified targeted protein (i.e. SPRED1 and GSK3) was incubated with active AKT recombinant protein and 10 µCi of [γ-^{32}] ATP (PerkinElmer Life Sciences) in 50 µl of kinase buffer. Reactions were incubated at 30°C for 1 hour. Protein complex was then separated on NUPAGE 4-12% gradient gels (Thermo Scientific, Lafayette, CO). The gel was then dried, and the phosphorylated protein was visualized by autoradiography. The information of used proteins for kinase assay is listed in Table S4.

miRNA labeling and analysis with SmartFlare probes

MiRNAs were labeled and analyzed with SmartFlare probes as described before (1,2). The lyophilized SmartFlare probes for miR-126 and miR-155 and uptake, scramble or 18S housekeeping control (EMD Millipore) were reconstituted with 50 µl of nuclease free water and kept at room temperature. MV-4-11 and primary AML blasts (treated or non-treated) were plated in a 96 well plate (30,000 cells/well) in 200 µl of media. Working solution of each SmartFlare probe was prepared by diluting 1:20 with PBS. Then, 4 µl of working solution was added into 200 µl of media with 30,000 cells in a single well of a 96-well plate to get the concentration of 100 pM. The cells were plated in 37^0C, 5% CO_2 for 16 hours. Cells were then washed in 1× PBS and fixed in 4% paraformaldehyde for 3 min. Nuclei were counterstained with DAPI, and the images were analyzed using a confocal microscope (Zeiss LSM880). To ensure that the cell types, including MV-4-11 and primary AML blasts, were able to effectively endocytose the SmartFlare probes, we examined the uptake of probes in these cells using a SmartFlare uptake control, a scrambled control and a housekeeping 18S control (according to the manufacturer's guidelines) (3,4).

Mathematic model of FLT3-ITD regulated miR-126 and miR-155

Mathematical model of FLT3-ITD regulated cell proliferation through controlling dynamics of miRNA circuits such as miR-126 and miR-155 is represented by the circuit in Figure 6A. The activation of FLT3-ITD (X) is assumed to increase from an initial value X_0 to a final value X_f in a continuous and smooth fashion. The activation of X is therefore modeled by the equation in Figure 6B where the parameters σ and ϕ determine the velocity and the time at which the activation takes place, respectively.

The evolution in time of the compartments T_1, T_2, T_3, T_4, Y_1, and Y_2 is determined by assuming the law of mass action. With this assumption, the interaction between two compartments e.g., A and

B, is directly proportional to their product e.g., AB: the constant of proportionality is positive if e.g. A activates B and is negative if e.g., A inhibits B. Moreover, each compartment has a natural death rate proportional to itself and a natural production rate. With these prescriptions, the evolution in time of all compartments is modeled in Figure 6B where the dot on top of the variables on the left hand side represent the time derivative, the positive parameters α, β, γ, δ, ε, η, κ, λ, μ, ρ, ξ quantify the interaction between the compartments, and Θ_i and Γ_i (i=1,…,6) are the constant death rate and the constant growth rate, respectively. Finally, the leukemic growth Z is assumed to follow a logistic law with a carrying capacity K and a constant growth rate ν described by the second-to-last equation in Figure 6B.

The time evolution of all compartments in the circuit is indeed obtained by numerically solving the set of ordinary differential equations (ODEs). In particular, we used the built-in ODE45 Matlab solver based on an adaptive 4^{th}-5^{th} order Runge-Kutta scheme and the results are shown in Figure 6B.

Supplementary References

1. Zhang, B., Nguyen, L. X. T., Li, L., Zhao, D., Kumar, B., Wu, H., Lin, A., Pellicano, F., Hopcroft, L., Su, Y. L., et al. (2018). Bone marrow niche trafficking of miR-126 controls the self-renewal of leukemia stem cells in chronic myelogenous leukemia. Nat. Med. *24*, 450-462.

2. Nguyen, L.X.T., Zhang, B., Hoang, D.H., Zhao, D., Wang, H., et al. (2021). Cytoplasmic DROSHA and non-canonical mechanisms of MiR-155 biogenesis in FLT3-ITD acute myeloid leukemia. Leukemia 10.1038/s41375-021-01166-9.

3. Lahm H, Doppler S, Dressen M, Werner A, Adamczyk K, Schrambke D, et al. (2015) Live fluorescent RNA-based detection of pluripotency gene expression in embryonic and induced pluripotent stem cells of different species. Stem Cells 33, 392-402.

4. McClellan S, Slamecka J, Howze P, Thompson L, Finan M, Rocconi R, et al. (2015). mRNA detection in living cells: A next generation cancer stem cell identification technique. Methods 82, 47-54.

Supplementary Table 1. The target sequences for siRNAs

No	Name	Target Sequence
1	siAKT1	CAUCACACCACCUGACCAA ACAAGGACGGGCACAUUAA CAAGGGCACUUUCGGCAAG UCACAGCCCUGAAGUACUC

Supplementary Table 2. TaqMan gene expression assays used for qPCR analysis

No	Gene name	Assay ID
1	hsa-miR-126-5p	477888_mir
2	hsa-miR-126-pri	Hs03303230_pri
3	hsa-miR-155-3p	477926_mir
4	mmu-miR-126a-5p	mmu480908_mir
5	mmu-miR-155-3p	mmu481328_mir

Supplementary Table 3. List of antibodies used for IP and IB analysis

No	Antibody name	Information
1	Anti-SPRED1 antibody	Clone# M23-P2G3, Cat# ab64740, ABCAM, RRID:AB_2270978
2	Anti-AKT antibody	Cat# 9272, Cell Signaling, RRID:AB_329827
3	Anti-GSK-3 antibody	Clone# D75D3, Cat# 5676, Cell Signaling, RRID: AB_2737080
4	Anti-RAN antibody	Cat# ab4781, ABCAM, RRID:AB_304618
5	Anti-ACTIN antibody	Clone# C4, Cat# sc-47778, Santa Cruz, RRID:AB_2737082

6	Anti-HA antibody	Cat# sc-7392, Santa Cruz, RRID:AB_627809
7	Anti-GFP antibody	Cat# sc-8334, Santa Cruz, RRID:AB_641123
8	Anti-DDX3X antibody	Cat# NBP1-85291, Novus Biologicals, RRID:AB_11034160
9	Anti-p-S/T antibody	Cat# 9631, Cell Signaling, RRID:AB_330308
10	Anti-SHIP1 antibody	Clone# D1163, Cat# 2728, Cell Signaling, RRID:AB_2126244
11	Anti-p-AKT (Ser473) antibody	Cat# 9271, Cell Signaling, RRID:AB_329825

Supplementary Table 4. List of proteins used for *in vitro* kinase assay

No	Protein name	Information
1	Active AKT protein	Cat# 14-453, EMD Millipore
2	SPRED1 protein	Cat# NBP2-51864, Novus Biologicals
3	GSK3 protein	Cat# 9237, Cell Signaling

Supplementary Table 5. Characteristics of patient samples

Sample Number	Sample Type	Disease Status	Cytogenetic	Gene Mutation								WBC (10^3/µl)	PB Blasts (%)	BM Blasts (%)
				FLT3-ITD	FLT3-TKD	FLT3-D853	NPM1	CEBPA	C-KIT	IDH1	IDH2			
AML01	PB	Untreated	Normal	Pos	Neg	Neg	Neg	Pos	Neg	Neg	Neg	76.8	84	75
AML02	BM	Refractory	Complex	Pos	Neg	Neg	Pos	Neg	Neg	Neg	Neg	4.2	91	90
AML03	PB	Untreated	Normal	Pos	Neg	Neg	Neg	Neg	Neg	Neg	Neg	22	83	90
AML04	BM	Relapsed	Normal	Pos	Neg	Neg	Pos	Neg	Neg	Neg	Neg	101.7	93	95
AML05	BM	Relapsed	Complex	Pos	Neg	Neg	Pos	Neg	Neg	Neg	Neg	46.4	90	>90
AML06	BM	Relapsed	Normal	Pos	Neg	Neg	Neg	Neg	Neg	Neg	Neg	15	6	19
AML07	BM	Untreated	Complex	Pos	Neg	Neg	Pos	Neg	Neg	Neg	Neg	68.3	73	96
AML08	PB	Relapsed	Complex	Pos	Neg	Neg	Pos	Neg	Neg	Neg	Neg	46.4	66	>90
AML09	PB	Relapsed	Normal	Pos	Neg	Neg	Pos	Neg	Neg	Neg	Neg	10.9	76	53
AML10	PB	Relapsed	Normal	Pos	Neg	Neg	Pos	Neg	Neg	Neg	Neg	16.3	48	70

AML11	PB	Untreated	Normal	Neg	Neg	Neg	Pos	Neg	Neg	Neg	Neg	33	87	90
AML12	PB	Untreated	Normal	Neg	Neg	Neg	Neg	Neg	Neg	Neg	Neg	29	91	>90
AML13	PB	Untreated	Normal	Neg	Neg	Neg	Neg	Neg	Neg	Neg	Neg	11.6	81	36
AML14	BM	Untreated	Normal	Neg	Neg	Neg	Pos	Neg	Neg	Neg	Neg	20.7	59	90
AML15	PB	Untreated	Normal	Neg	Neg	Neg	Neg	Pos	Neg	Neg	Neg	33	80	60
AML16	BM	Relapsed	Normal	Neg	Neg	Neg	Neg	Neg	Neg	Neg	Neg	0.6	8	80
AML17	BM	Refractory	13q deletion	Neg	Neg	Neg	Neg	Neg	Neg	Neg	Neg	3.9	0	35
AML18	BM	Untreated	Normal	Neg	Neg	Neg	Neg	Neg	Neg	Neg	Pos	1.2	30	>90

AML19	BM	Untreated	Normal	Neg	Neg	Neg	Neg	Neg	Neg	Neg	Pos	1.4	5	>90
AML20	PB	Relapsed	Complex	Neg	Neg	Neg	Pos	Neg	Neg	Neg	Neg	23.2	31	72
AML21	BM	Untreated	Complex	Pos	Neg	Neg	Neg	Neg	Neg	Neg	Neg	1.5	0	26
AML22	BM	Relapsed	Complex	Pos	Neg	Neg	Pos	Neg	Neg	Neg	Neg	46.4	66	>90
AML23	BM	Untreated	Complex	Pos	Neg	Neg	Neg	Neg	Neg	Neg	Neg	2.8	0	6
AML24	BM	Untreated	Complex	Pos	Neg	Neg	Neg	Neg	Neg	Neg	Neg	62.3	88	90
AML25	PB	Relapsed	Normal	Pos	Neg	Neg	Neg	Neg	Neg	Neg	Neg	23.5	36	60

Supplementary Table 6. Mathematical model parameters and initial conditions

Numerical integration of the system of ordinary differential equations described in Eq. 8 was performed using the reported parameters. The parameter dimensional units and values are reported at the two-digit significance level. Concentration, time, and the number of cells is represented by C, T, and cell, respectively. The set of parameters reported here and used in the model were estimated to show that the dependency structure encoded in the interaction schematic (Figure 6). The corresponding mathematical equations were qualitatively consistent with the experimental evidence. Initial conditions were as follows: $T_{1-4}(0) = Y_{1-2}(0) = 0$ and $Z(0) = 0.5, X(0) = 1$. The model parameters were estimated based on rates of reactions relative to the timescale of leukemia growth and relative proportions of concentrations at steady-state in the presence and absence of FLT3-ITD.

symbol	value	unit	description
α	0.17	$C^{-1}T^{-1}$	Interaction constants
β	0.35	$C^{-1}T^{-1}$	
γ	1.21	$C^{-1}T^{-1}$	
δ	0.3	$C^{-1}T^{-1}$	
ε	0.23	$C^{-1}T^{-1}$	
ζ	0.46	$C^{-1}T^{-1}$	
η	2.2×10^{-3}	$C^{-1}T^{-1}$	
κ	1.61	$C^{-1}T^{-1}$	
λ	0.87	$C^{-1}T^{-1}$	
μ	1.7	$C^{-1}T^{-1}$	
ν	0.56	T^{-1}	
ρ	0.56	$C^{-1}T^{-1}$	
Θ_1	1.37	T^{-1}	Degradation rate
Θ_2	0.15	T^{-1}	
Θ_3	1.71	T^{-1}	
Θ_4	0.0	T^{-1}	
Θ_5	0.0	T^{-1}	
Θ_6	0.0	T^{-1}	
Γ_1	1.25	$C\ T^{-1}$	Production rate
Γ_2	1.27	$C\ T^{-1}$	
Γ_3	1.11	$C\ T^{-1}$	
Γ_4	0.75	$C\ T^{-1}$	
Γ_5	0.6	$C\ T^{-1}$	
Γ_6	0.6	$C\ T^{-1}$	

K	3.15	cell	Carrying capacity

Supplementary Figure Legends

Figure S1. Specificity of SmartFlare probes. MiR-126 and miR-155 were overexpressed or knocked down in MV-4-11 cells and the cells were stained with specific SmartFlare probe for each miRNA. Staining images are shown on the left and relative PCR results are on the right.

Figure S2. Effects of AC220 treatment *in vivo* on levels of miR-126 and miR-155. The BM cells from FLT3-ITD+ AML patients pre- or post-treated with AC220 (n=4) were collected to analyze as indicated. Levels of miR-126 and miR-155 as measured by q-PCR (A) and staining with SmartFlares miRNA probes (B).

Figure S3. Effects of AC220 and K118-SHIP1 inhibitor on levels of miR-126 and apoptosis. (A and B) Effects of miR-155 inhibition on SHIP1/p-AKT/SPRED1 signaling and miR-126 expression. HL-60 cells (A) or Lin- BM cells from normal wt mice (B) were treated with either miR-126 inhibitor or miR-155 inhibitor alone or combination for 24 hours. Left, expression levels of miR-126 and miR-155 by q-PCR. Right, cell lysate was immunoblotted with indicated antibodies. (C) Left, MV-4-11 cells were transfected with siSCR or siSHIP1 (20 and 40 nM) for 24 hours and miR-126 was examined. Middle and right, the cells were treated with either AC220 (0.5 nM) or K118 (10 μM) alone, or combination of these inhibitors for 24 hours. Levels of miR-126 and apoptosis are shown.

Figure S4. Effects of AKT phosphorylation on SPRED1 stabilization and localization. (A and B) Interaction of AKT and SPRED1 in Lin- BM cells from *Mll*$^{PTD/wt}$/*Flt3*$^{ITD/ITD}$ AML mice (A) and HL-60 cells (B). (A) Protein lysate from Lin- BM cells from *Mll*$^{PTD/wt}$/*Flt3*$^{ITD/ITD}$ AML mice were immunoprecipitated with anti-IgG or anti-AKT antibody and immunoblotted with anti-SPRED1

antibody. (B) HL-60 cells were transfected with HA-AKT and GFP-SPRED1 and immunoprecipitation and immunoblotting were performed as shown. (C) Cellular distribution of SPRED1 WT and SPRED1 S238A (non-AKT-phosphorylated mutation) in Lin- BM cells from *Mll*$^{PTD/wt}$/*Flt3*$^{ITD/ITD}$ AML mice (left) and HL-60 cells (right). Indicated transfected cells with SPRED1 WT and SPRED1 S238A were fractionated and immunoblotted with indicated antibodies. (D) Interaction between SPRED1 WT and SPRED1 S238A with RAN. Lin- BM cells from *Mll*$^{PTD/wt}$/*Flt3*$^{ITD/ITD}$ AML mice (left) and HL-60 cells (right) were transfected with HA-RAN and GFP-SPRED1 WT or GFP-SPRED1 S238A. Immunoprecipitation and immunoblotting as shown. (E) Different half-life expression of SPRED1 WT and SPRED1 S238A. MV-4-11 cells were transfected with GFP-SPRED1 WT or GFP-SPRED1 S238A for 24 hours and continuously treated with CHX on time course. Cell lysate was immunoblotted with anti-GFP and anti-ACTIN antibodies. (F and G) Effects of AKT inhibition on SPRED1 localization. MV-4-11 cells were treated with DMSO control or AKT inhibitors (AZD8055, AKTi viii, or MK2206) for 24 hours. Fractionated lysate was immunoblotted with indicated antibodies (F). The treated cells were stained with SPRED1 and RAN (G). (H) Effect of AKT KD and OE on SPRED1 ubiquitination. FLT3-ITD+ AML blasts were co-transfected with HA-Ubiquitin and siSCR or siAKT (left) and GFP vector or GFP-AKT (right) for 24 hours. Ubiquitination assay was performed with anti-SPRED1, anti-GFP and anti-HA-Ubiquitin antibodies. (I) Effect of AKT KD and OE on protein stability of SPRED1. FLT3-ITD+ AML blasts were transfected with siSCR and siAKT (top) or HA vector control and HA-AKT (bottom) for 24 hours. Lysate from indicated transfected cells were immunoblotted with anti-SPRED1, anti-AKT and anti-ACTIN antibodies. (J) Effect of AKT KD on SPRED1 protein stability. FLT3-ITD+ AML blasts were transfected with siSCR or siAKT for 24 hours. The cells were then treated with CHX (10 μM) for the indicated times and lysate was immunoblotted with indicated antibodies.

Figure S5. Effects of FLT3 activation on miR-155-regulated miR-126 levels. (A) Effects of FLT3-ITD overexpression on SPRED1/AKT interaction in HL-60 cells. Protein lysate from control or FLT3-ITD infected HL-60 cells was immunoprecipitated with anti-AKT antibody and immunoblotted with anti-SPRED1 antibody. Input control was shown. (B) Effects of AC220 treatment *in vivo* on SPRED1 localization. The BM cells from FLT3-ITD+ AML patients pre- or post-treated with AC220 (n=4) were collected and stained with anti-SPRED1 and anti-RAN antibodies. Scale bar, 10 μm. (C) and (D) Effects of FLT3 activation on miR-155-regulated miR-126 levels. (C) FLT3 wt THP1 cells and FLT3-ITD MV-4-11 cells were treated with FLT3 ligand (100 ng/ml) for 24 h. Left, levels of miR-155 and miR-126 measured by q-PCR. Middle, cell lysate was immunoblotted with indicated antibodies. Right, densitometry quantification of immunoblotting. (D) CD34+ normal PBSC, FLT3 wt and FLT3-ITD AML blasts (each, n=3) were treated with FLT3 ligand (100 ng/ml) for 24 h. Top, levels of miR-155 and miR-126 measured by q-PCR. Bottom, cell lysate was immunoblotted with indicated antibodies (left) and densitometry quantification of immunoblotting (right).

Figure S6. Schematic model of FLT3-ITD-caused a deregulated "circuitous architecture" of the miRNome in AML. FLT3-ITD inputs a signal that leads to concurrent miR-126 down- and miR-155 up-regulation in AML blasts. FLT3-ITD downregulates miR-126 expression through a miR-126-SPRED1 negative "feedback loop" in which SPRED1, a downstream target of miR-126, inhibits the miRNA biogenesis "gatekeeper" complex XPO5-RAN-GTP and blocks miR-126 maturation (left). In parallel, FLT3-ITD also upregulates miR-155 expression through a miR-155-DDX3X negative "feedback loop" in which altered levels of DDX3X, a downstream target of miR-155, disrupt the splicing of the lnc-RNA BIC-155, thereby allowing previously unreported NXF1-mediated transport of unspliced BIC-155 to feed into cytoplasmic DROSHA activity and enhance mature miR-155 synthesis, thereby circumventing the XPO5-RAN-GTP blockage (right). These two "feedback loops" are interconnected through a "feedforward loop" generated by a direct

regulatory role of miR-155 on miR-126 expression through modulation of the SHIP1-AKT signaling (bottom). This complex circuit of interconnected loops eventually converge to a common output signal for leukemia growth that can be therapeutically targeted.

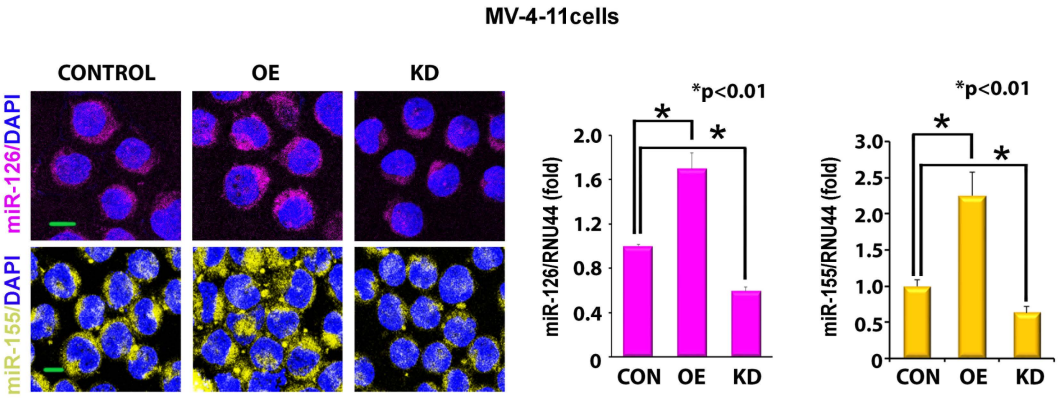
MV-4-11cells
CONTROL
OE
KD
miR-126/DAPI
miR-155/DAPI
*p<0.01
miR-126/RNU44 (fold)
2.0
1.6
1.2
0.8
0.4
0
CON
OE
KD
*p<0.01
miR-155/RNU44 (fold)
3.0
2.5
2.0
1.5
1.0
0.5
0
CON
OE
KD

Figure S1

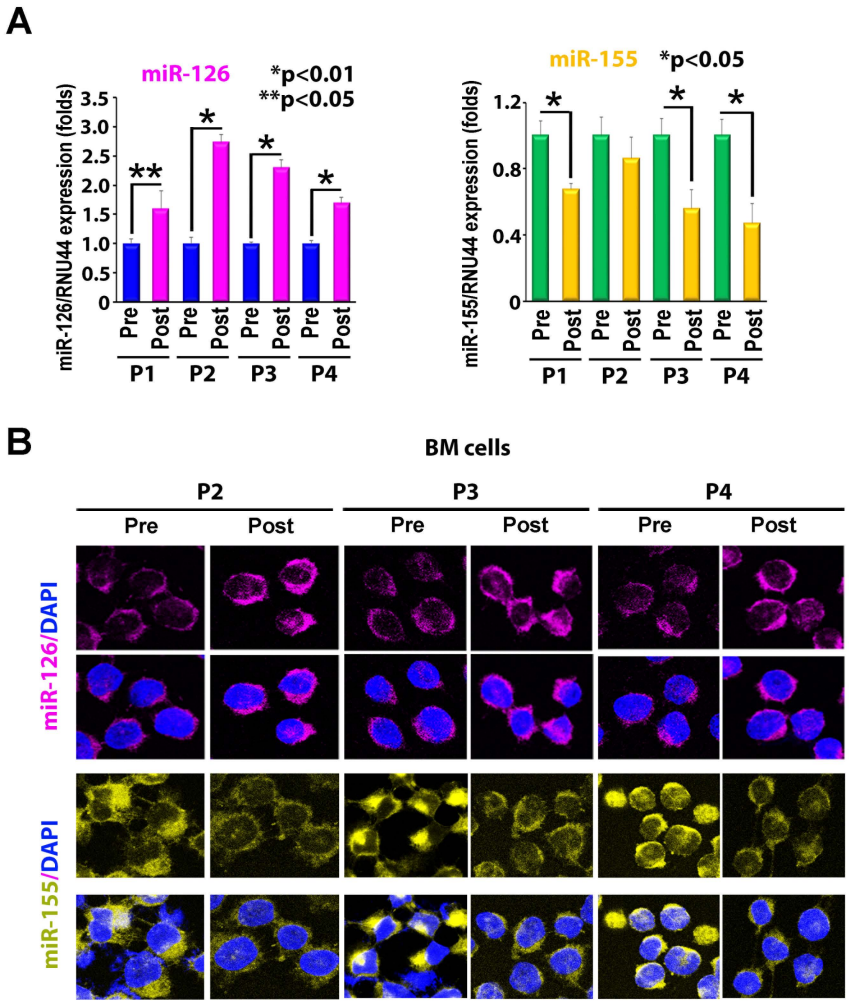
A
miR-126
*p<0.01
**p<0.05
miR-126/RNU44 expression (folds)
3.5
3.0
2.5
2.0
1.5
1.0
0.5
0
**
*
*
*
Pre
Post
P1
P2
P3
P4
miR-155
*p<0.05
miR-155/RNU44 expression (folds)
1.2
0.8
0.4
0
*
*
*
B
BM cells
P2
P3
P4
Pre
Post
miR-126/DAPI
miR-155/DAPI

Figure S2

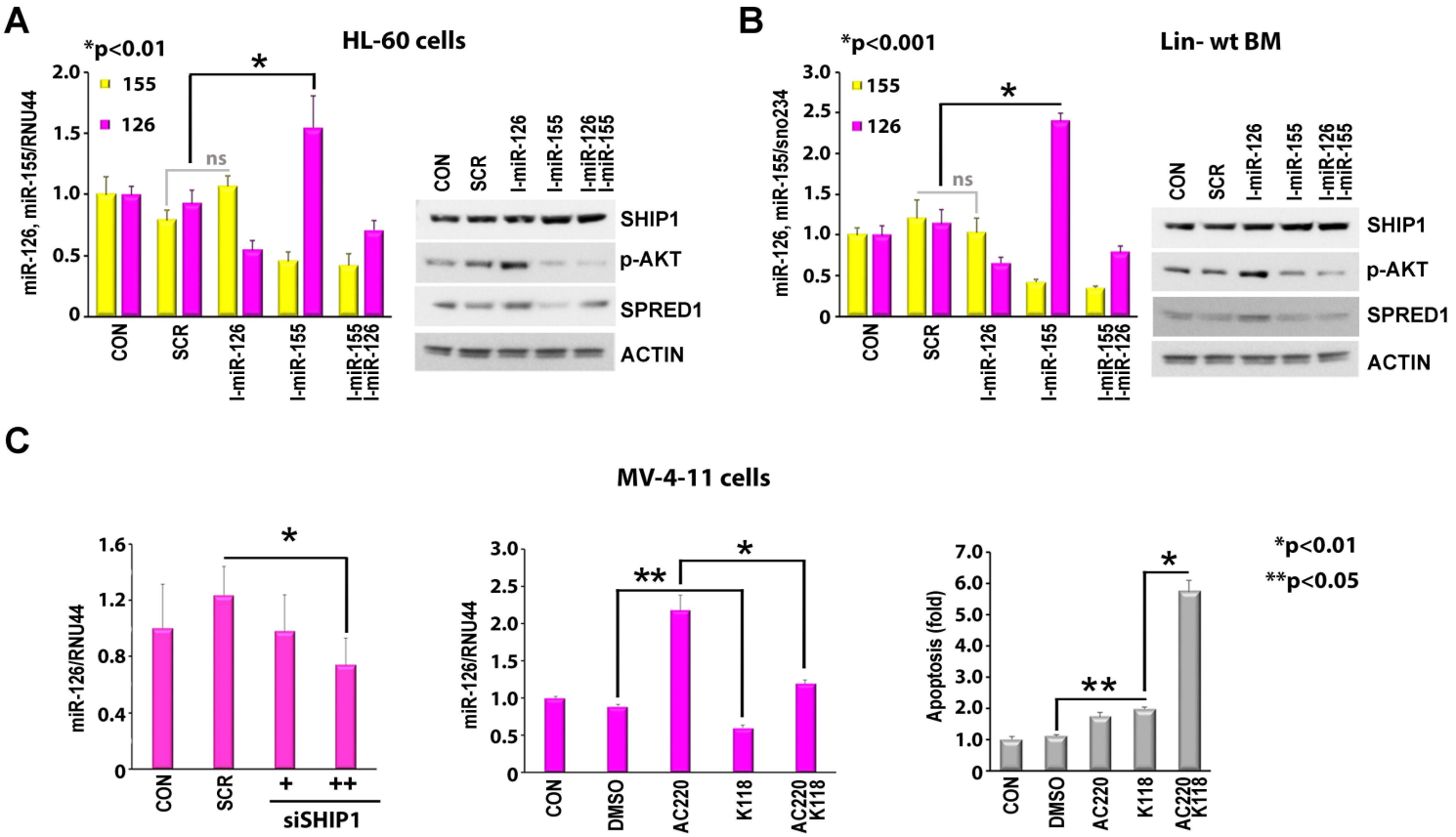
A
*p<0.01
HL-60 cells
155
126
ns
miR-126, miR-155/RNU44
CON
SCR
l-miR-126
l-miR-155
l-miR-155 l-miR-126
SHIP1
p-AKT
SPRED1
ACTIN
B
*p<0.001
Lin- wt BM
miR-126, miR-155/sno234
C
MV-4-11 cells
miR-126/RNU44
siSHIP1
DMSO
AC220
K118
AC220 K118
Apoptosis (fold)
*p<0.01
**p<0.05

Figure S3

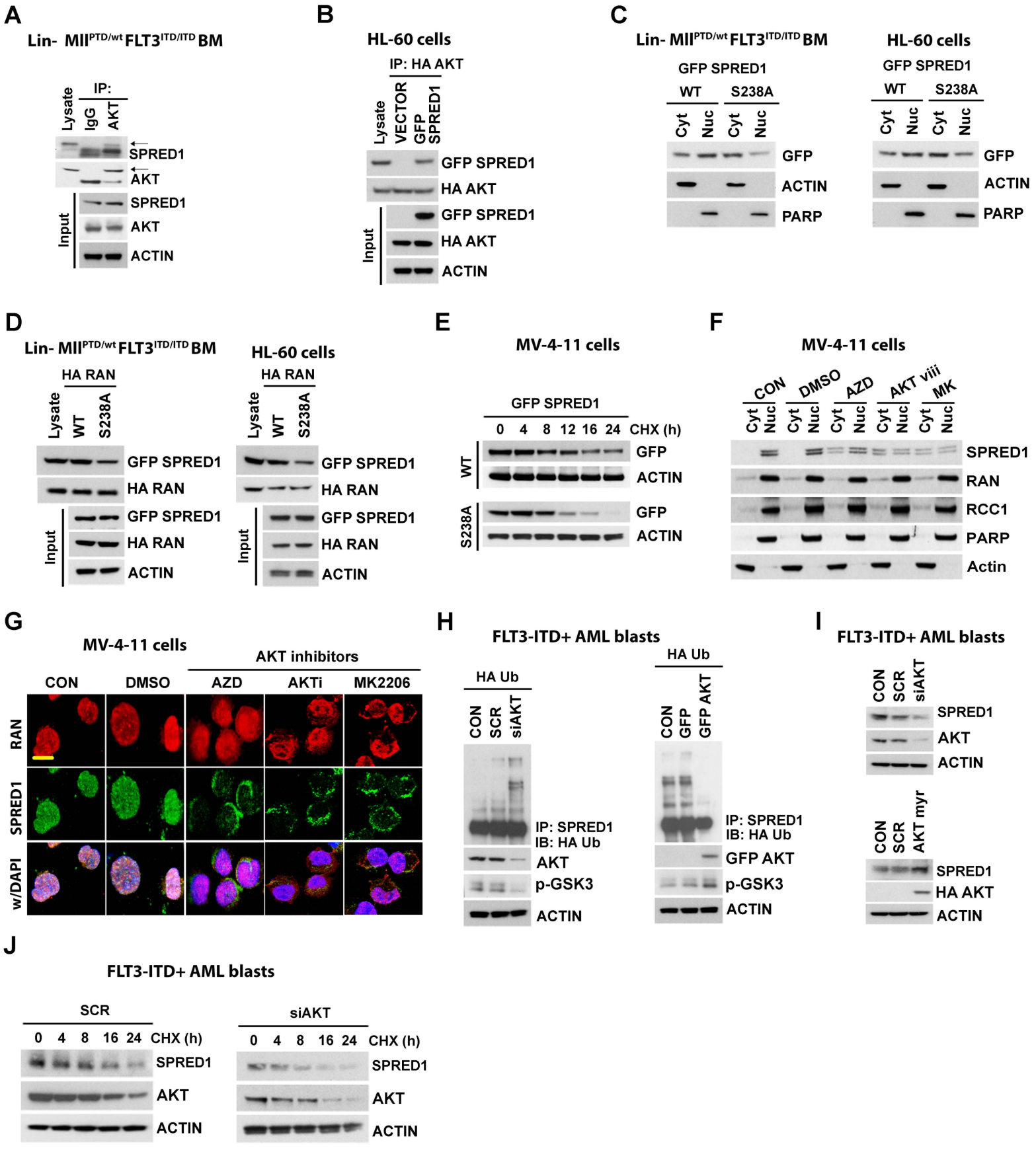
A
Lin- MllPTD/wt FLT3ITD/ITD BM
Lysate
IP:
IgG
AKT
SPRED1
AKT
Input
SPRED1
AKT
ACTIN
B
HL-60 cells
IP: HA AKT
Lysate
VECTOR
GFP SPRED1
GFP SPRED1
HA AKT
Input
GFP SPRED1
HA AKT
ACTIN
C
Lin- MllPTD/wt FLT3ITD/ITD BM
HL-60 cells
GFP SPRED1
WT
S238A
Cyt
Nuc
GFP
ACTIN
PARP
D
Lin- MllPTD/wt FLT3ITD/ITD BM
HL-60 cells
HA RAN
Lysate
WT
S238A
GFP SPRED1
HA RAN
Input
ACTIN
E
MV-4-11 cells
GFP SPRED1
0 4 8 12 16 24 CHX (h)
WT
S238A
GFP
ACTIN
F
MV-4-11 cells
CON
DMSO
AZD
AKT viii
MK
SPRED1
RAN
RCC1
PARP
Actin
G
MV-4-11 cells
AKT inhibitors
CON
DMSO
AZD
AKTi
MK2206
RAN
SPRED1
w/DAPI
H
FLT3-ITD+ AML blasts
HA Ub
CON
SCR
siAKT
GFP
GFP AKT
IP: SPRED1
IB: HA Ub
AKT
p-GSK3
ACTIN
I
FLT3-ITD+ AML blasts
CON
SCR
siAKT
AKT myr
SPRED1
AKT
HA AKT
ACTIN
J
FLT3-ITD+ AML blasts
SCR
siAKT
0 4 8 16 24 CHX (h)
SPRED1
AKT
ACTIN

Figure S4

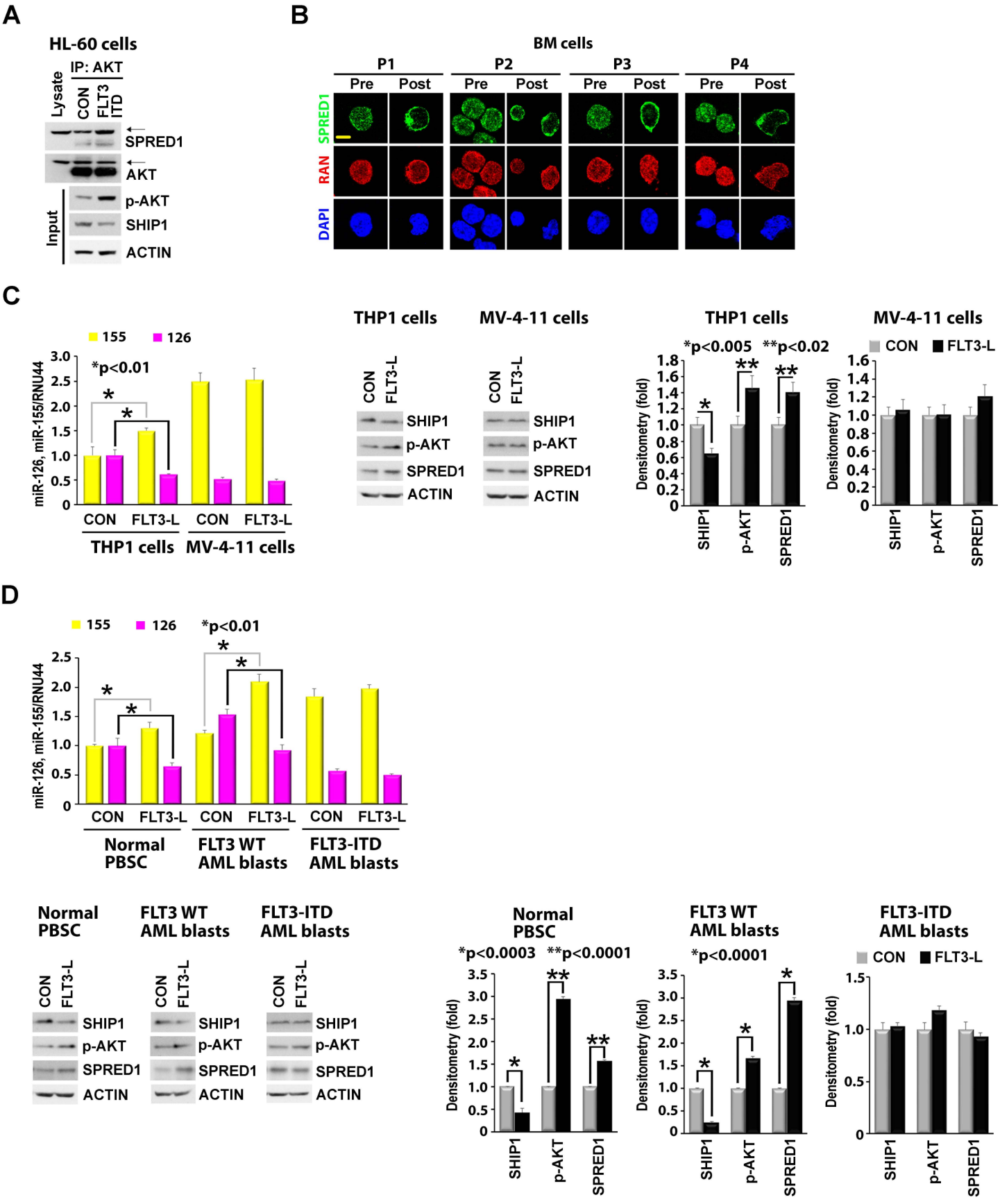
A
HL-60 cells
IP: AKT
Lysate
CON
FLT3 ITD
SPRED1
AKT
Input
p-AKT
SHIP1
ACTIN
B
BM cells
P1
P2
P3
P4
Pre
Post
SPRED1
RAN
DAPI
C
155
126
*p<0.01
miR-126, miR-155/RNU44
CON
FLT3-L
THP1 cells
MV-4-11 cells
SHIP1
p-AKT
SPRED1
ACTIN
*p<0.005
**p<0.02
Densitometry (fold)
D
*p<0.0003
**p<0.0001
*p<0.0001
Normal PBSC
FLT3 WT AML blasts
FLT3-ITD AML blasts

Figure S5

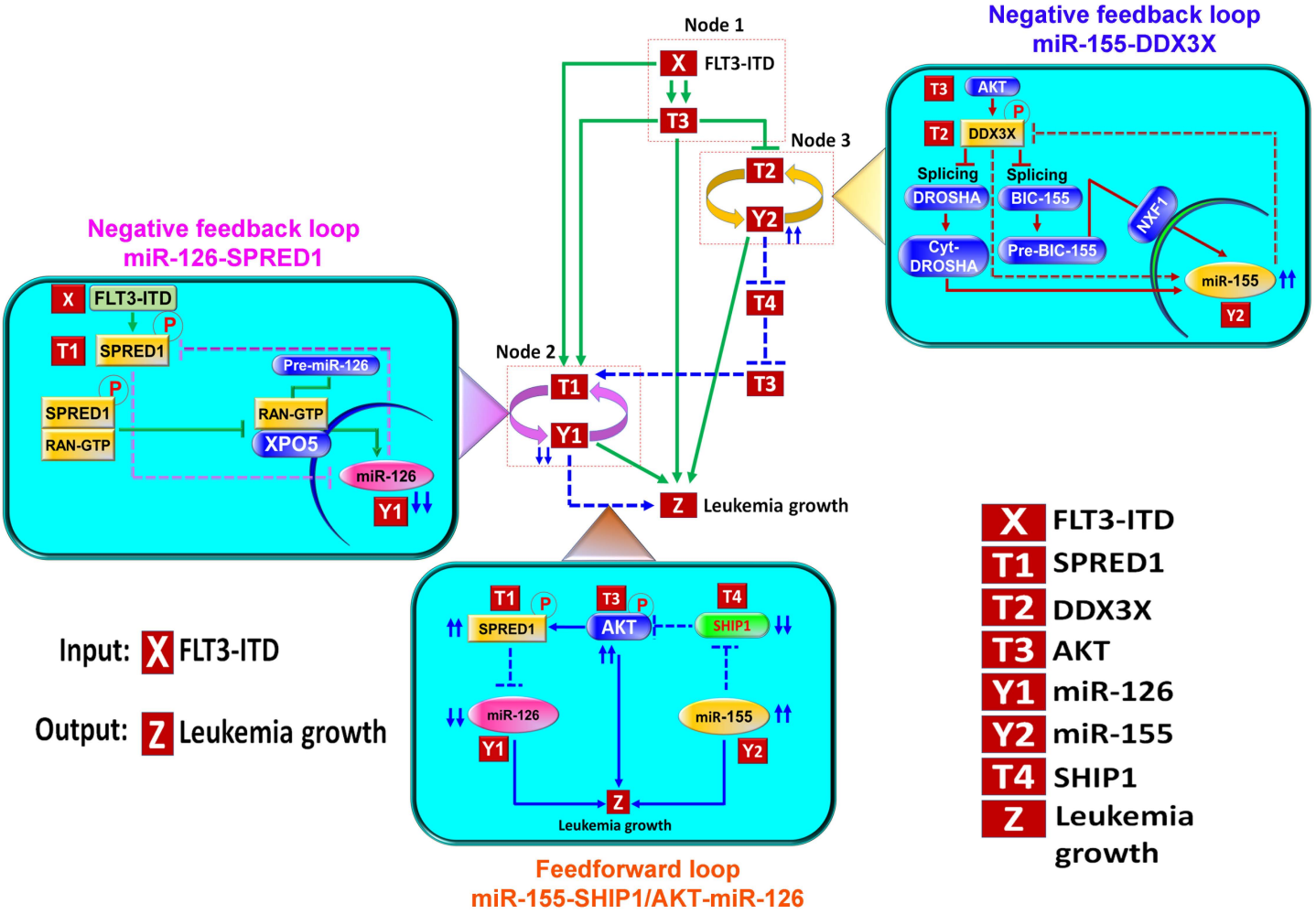
Node 1
X FLT3-ITD
T3
Node 3
T2
Y2
T4
T3
Node 2
T1
Y1
Z Leukemia growth
Negative feedback loop
miR-126-SPRED1
X FLT3-ITD
P
T1 SPRED1
Pre-miR-126
P
SPRED1
RAN-GTP
RAN-GTP
XPO5
miR-126
Y1
Negative feedback loop
miR-155-DDX3X
T3 AKT
P
T2 DDX3X
Splicing
Splicing
DROSHA
BIC-155
NXF1
Cyt-DROSHA
Pre-BIC-155
miR-155
Y2
Input: X FLT3-ITD
Output: Z Leukemia growth
T1 P
T3 P
T4
SPRED1
AKT
SHIP1
miR-126
miR-155
Y1
Y2
Z
Leukemia growth
Feedforward loop
miR-155-SHIP1/AKT-miR-126
X FLT3-ITD
T1 SPRED1
T2 DDX3X
T3 AKT
Y1 miR-126
Y2 miR-155
T4 SHIP1
Z Leukemia growth

Figure S6